Journal of New Technology and Materials (JNTM)
J. New Technol. Mater.
Vol. 08, N°01 (2018)58-67

OEB Univ. Publish. Co.

Developing heat transfer in a solar air channel with arc-shaped baffles: effect of baffle attack angle

Younes Menni[a,*], Ahmed Azzi[a,b] and Ali J. Chamkha[c,d]

[a]*Unit of Research on Materials and Renewable Energies - URMER -Department of Physics, Faculty of Sciences,Abou Bekr Belkaid University, BP 119 - 13000 - Tlemcen – Algeria*

[b]*Department of Mechanical Engineering, Faculty of Technology,Abou Bekr Belkaid University,BP 230 - 13000 - Tlemcen – Algeria*

[c]*Mechanical Engineering Department, Prince Sultan Endowment for Energy and Environment, Prince Mohammad Bin Fahd University, Al-Khobar 31952, Saudi Arabia*

[d]*RAK Research and Innovation Center, American University of Ras Al Khaimah, United Arab Emirates*

*Corresponding author (Dr Younes Menni): email: menniyounes.cfd@gmail.com

Received date: Jan. 05, 2018; revised date: Apr. 05, 2018; accepted date: Apr. 10, 2018

Abstract

The current study illustrates a computational fluid dynamic analysis of 2D steady-state turbulent forced-convection flow and friction loss characteristics through a constant temperature-surfaced rectangular cross section channel fitted with two staggered, upper and lower wall-attached, arc-shaped, solid-type obstacles. The aspect ratio of channel width-to-height, channel length-to-aeraulic diameter, baffle spacing-to-channel height ratio, and blockage ratio of baffle height-to-channel height are fixed at W/H = 1.321, L/D_h = 3.317, Pi/H = 0.972, and h/H = 0.547, respectively. The numerical runs were carried out for various attacks of arc-baffle angle values, θ = 30°, 45°, 60°, and 75°, at constant surface temperature condition along the upper and lower channel walls. In particular, fields of mean velocity, profiles of axial velocity, local and average distributions of Nusselt numbers, and skin friction loss were obtained for a constant value of the flow Reynolds number. The numerical result analysis showed that the value of arc-baffle angle of attack of flow plays an important role in fluid flow as well as thermal heat behaviors and also impacts skin friction loss.

Keywords: Arc-shaped obstacles; Computational fluid; Friction loss; Rectangular channel; Solar energy collectors.

1. Introduction

The heat transfer enhancement technique by inserting baffles and fins in the fluid flow field domain has been the subject of many numerical and experimental studies. Berner et al. [1] used the Laser Doppler Anemometry (LDA) technique to get some experimental values of the average velocity and turbulence distributions in the turbulent regime throughout a duct with many segmented baffle plates. The authors aimed at determining the number of baffles that are needed to have the periodic boundary condition and to determine the relationship between the flow rate and the geometry.

Cheng and Huang [2] conducted a computational analysis on the laminar flow forced-convection in parallel-plate channels supplied with two series of transversal fins. The results they obtained showed that the position of one fin array with respect to the other is a factor that greatly influences the flow field, particularly for the cases of high fins and in general the in-line arrangement behaves in effectively due to the remarkable flow recirculation covering the wall surfaces.

Li and Kottke [3] studied the convective heat transfer and friction loss in simulating models of shell-and-tube heat exchangers. Parameters of the experimental work were the Reynolds number and the distance between the baffles. Results demonstrated that for a constant value of the Reynolds number, increasing the distance between the baffles increased the heat exchange coefficient and the pressure drop.

A numerical and experimental study was carried out by Demartini et al. [4] on air flow inside a channel with a rectangular cross section with two baffle plates mounted on the upper and lower walls. This study included also a comprehensive investigation of the velocity and pressure profiles. The solution to the problem was found by the Hot Wire Anemometry technique and the Finite Volume method using the commercial program Fluent 5.2.

Mousavi and Hooman [5] carried out numerical simulations of the laminar fluid flow and heat transfer in a two dimensional horizontal channel containing staggered solid baffles and fins. Various geometrical parameters of the model and different operating parameters were considered in that study.

Antoniou and Bergeles [6] analyzed the flow over a prism with several aspect ratios using hot wire technique. By increasing the aspect ratio *L/H*, the flow reattaches on the prism surface and downstream, while recirculation lengths and turbulence scales are reduced.

Experimental results of velocity and wall pressure fluctuations in the turbulent flow through a simulated tube bank with square arrangement, after passing a baffle plate were performed by Möller et al. [7], using hot wires and a pressure transducer. Behavior of fluctuating quantities was described by means of dimensionless autospectral density functions and their interdependence was discussed.

Nasiruddin and Kamran Siddiqui [8] indicated that the convective heat transfer in a heat exchanger tube may be enhanced by placing a baffle inside the tube. The investigators considered a comparative study between three different baffle orientations. The first case examined a vertical baffle. The second case investigated a baffle inclined towards the upstream end, and the third one considered a baffle inclined towards the downstream end. The results suggested that a baffle inclined towards the downstream side with a smaller inclination angle (15° in their study) is a better choice as it enhances the heat transfer by a similar magnitude with a minimal pressure loss.

Yongsiri et al. [9] reported the results of numerical study of turbulent flow and heat transfer in a channel with inclined detached-ribs. In that study, the fluid flow, temperature field and thermal performance of the inclined detached-ribs with different attack angles (0 to 165°), were examined and compared with those of the typical transverse attached rib with the attack value of 90°. The computational results showed that, at high Reynolds number, the inclined ribs with attack angles of 60° and 120° yield comparable heat transfer rates and thermal performance factors which were higher than those given by the ones with other angles. On the other hand, at low Reynolds number, the effect of rib attack angle was insignificant.

In another experiment, Karwa and Maheshwari [10] investigated fully (open area ratio of 46.8%) and half (open area ratio of 26%) perforated baffles covering *Re* values ranging from 2,700 to 11,150. The study showed an enhancement of 79-169% in Nusselt number over the smooth duct for the fully perforated baffles and 133-274% for the half perforated baffles while the friction factor for the fully perforated baffles are 2.98-8.02 times of that for the smooth duct and is 4.42-17.5 times for the half perforated baffles. In general, the half perforated baffles are thermo-hydraulically better to the fully perforated baffles at the same pitch. Of all the configurations studied, the half perforated baffles at a relative roughness pitch of 7.2 give the greatest performance advantage of 51.6-75% over a smooth duct at equal pumping power.

Sahel et al. [11] presented a new baffle design to eliminate the formation of lower heat transfer areas (LHTAs), particularly in the downstream regions of solid-type baffles. This design concerns a perforated baffle having a row of four holes placed at three different positions. These positions are characterized by a ratio called the pore axis ratio (*PAR*) which is taken equal to 0.190, 0.425 or 0.660. In their study, the baffle perforated with *PAR* = 0.190 was found to be as the best design, which reduces significantly the LHTAs, since it ensures an increase in the thermal transfer rate from 2% to 65 %, compared with simple baffle. However, the pressure loss may decrease until 12 times compared with the simple baffle.

Dutta and Hossain [12] experimentally investigated the local heat transfer characteristics and the associated frictional head loss in a rectangular channel with inclined solid and perforated baffles. A combination of two baffles of same overall size was used in their experiment. The upstream baffle was attached to the top heated surface, while the position, orientation, and the shape of the other baffle were varied to identify the optimum configuration for enhanced heat transfer. A constant surface heat flux was applied from the top surface, but the bottom and the side surfaces were maintained at an adiabatic condition. The inline placement of baffles augments the overall heat transfer significantly by combining both jet impingement and the boundary layer separation. They also showed that the local Nusselt number distribution is strongly depended on the position, orientation, and geometry of the second baffle plate. For two inclined baffle cases (solid or perforated), the frictional head loss is much higher than that of a single baffle arrangement. Moreover, in two baffle cases, the friction factor ratio is larger if the second baffle is attached to the bottom plate instead of the top heated surface.

Guerroudj and Kahalerras [13] simulated the influence of porous block shape on the laminar mixed convective heat transfer and airflow characteristics inside a two-dimensional parallel plate channel when the buoyant and forced flow effects are simultaneously present. The influence of the buoyancy force intensity, the porous blocks shape going from the rectangular shape to the triangular shape, their height, the porous medium permeability, the Reynolds number and the thermal conductivity ratio was analyzed. The results revealed essentially, that the shape of the blocks can alter substantially the flow and heat transfer characteristics.

Sripattanapipat and Promvonge [14] simulated the laminar periodic flow and heat transfer in a two dimensional horizontal channel with isothermal walls and with staggered diamond-shaped baffles. They reported that the diamond shape of the baffle with different tip angles (5 to 35°) may enhance the heat transfer from 200 to 680% for Reynolds number ranging from 100 to 600. However, this intensification is associated with enlarged friction loss ranging from 20 to 220 times above the smooth channel.

Ben Slama [15] carried out experimental studies to visualize the air flow inside a flat-plate solar collector, using white smoke injected into the mobile air channel. This method shows the localization of the dead zones as well as the shape of vortices engendered by baffles. These baffles

were placed in the 25 mm thick mobile air channel located between insulator and the absorber. Five different solar air channel designs, namely, channel without baffles, channel with small baffles, channel with transversal baffles, channel with transversal and longitudinal baffles, and channel with delta wing-shaped baffles, were visualized in that study, which are referred as cases A, B, C, D, and E, respectively. For the case A, the author observed that there is a direct passage of the air in the medium of the channel, from the inlet towards the outlet. In addition, there are many dead zones. For the case B, the dead zones were located downstream of the baffles. It was remarkable to observe that their extent is considerable. For the case C, the author observed the formation of a meandering flow. In this case, it was clear that the length of the trajectory is more than double that of the channel, thus increasing the air speed and the heat transfer. On the other hand, the size of the dead zones was considerable. For the case D, the efficiency was very much increased, and in the case E, the delta wings, as indicated by the author, have the characteristic to form two vortices on their extrados. This depends on their opening and incidence angles.

Abene et al. [16] reported an experimental study, which consists of a solar energy simulation, to improve the thermal exchange between the fluid and the upper face of a solar air channel (SAC) by considering several types of obstacles: ogival transverse (OT), ogival inclined folded (OIF1), waisted tube (WT), waisted delta lengthways (WDL1) and waisted ogival lengthways (WOL1) disposed in rows in the dynamic air vein of the SAC. They proceeded to the application of the best two systems (WDL1) and transverse-longitudinal obstacles (TL) for drying an agricultural product grape. By comparing with the SAC without obstacles, the thermal transfers and, consequently, the output temperature and the thermal efficiency are clearly improved. The heat quantities and drying times obtained in the case of WDL1 are very important compared with the SAC without obstacles.

Tamna et al. [17] conducted an experimental and numerical study to examine the heat transfer and flow friction characteristics in a solar air heater channel fitted with multiple 45° V-baffle vortex generators (BVGs) at different pitch ratios (PRs) for the turbulent flow, Re from 4,000 to 21,000. Three BVG arrangements, namely, one BVG wall (or single BVG), in-line and staggered BVGs on two opposite walls were also investigated. The experimental result revealed that the smaller PR provides the highest heat transfer and friction factor for all BVGs. The in-line BVG yielded higher heat transfer and friction loss than the staggered and the single BVG. However, the single BVG with PR = 0.5 yielded the highest thermal performance.

Sriromreun et al. [18] reported experimental and numerical investigations of the heat transfer and flow friction characteristics for a solar air heater channel with in-phase and out-phase Z-shaped baffles in the turbulent regime from Re = 4,400 to 20,400. The Z-baffles inclined to 45° relative to the main flow direction are characterized at three baffle-to channel-height ratios (e/H = 0.1, 0.2 and 0.3) and baffle pitch ratios (P/H = 1.5, 2 and 3). The effects of e/H and P/H ratios were more significant for the in-phase Z-baffle than for the out-phase Z-baffle.

Nanan et al. [19] numerically and experimentally carried out a comparative investigation on the flow and heat transfer associated with baffle turbulators with different designs: typical straight baffles, straight cross-baffles, straight alternate-baffles, twisted-baffles, alternate twisted-baffles and twisted cross-baffles. The influence of pitch ratio from 1.0 to 2.0 and *Re* numbers from 6,000 to 20,000 were also examined. At the optimum condition of the smallest pitch ratio and the lowest Reynolds number, the twisted cross-baffles offered the highest thermal enhancement factor of 1.7.

Kumar et al. [20] experimentally examined the performance of heat transfer, friction factor and *TEF* in a solar air channel attached with 60° angled broken multiple V-type baffles with a *Re* ranging from 3,000 to 8,000. The baffle parameters were determined by baffle height (H_b), pitch of baffle (P_b), length of V-pattern baffle (L_s), Gap or discrete distance (D_b), Gap or discrete width (G_w), angle of attack (α_s), and the shape of the roughness elements. Effects of different relative baffle widths on the Nusselt number, pressure loss and overall thermal performance were studied. The obtained results showed that higher overall thermal performance occurred at a relative baffle width of 5.0. Also, the results showed that the broken multiple V-type baffles are thermo-hydraulically superior as compared to the other baffles shaped solar air channel.

Other similar works can be found in the literature (i.e., Menni et al. [21-23]; Menni and Azzi [24-26]; Merrouchi et al. [27]) that studied the heat transfer and fluid flow over baffles, fins, and plates submitted to turbulent forced-convection flows using different structural parameters and various operating regimes.

This manuscript presents a novel obstacle geometry that consists of an arc-shaped baffle having an angle of flow attack of four various values at constant surface temperature condition along the top and bottom walls. Our aim is to explore the impact of this configuration of obstacle on the thermal transfer rate and skin friction loss aspects inside a rectangular cross section channel by using the CFD code FLUENT.

2. Position of the Problem

2.1. Computational domain

The geometry under study is a two-dimensional constant temperature-surfaced rectangular cross section channel with an arc-shaped baffle pair placed on opposite positions of channel wall in a staggered manner as shown in Fig.1. The first arc-baffle is mounted on the upper wall of the channel and the second one is mounted on the lower wall. The structural parameters are based on the numerical and experimental work of Demartini et al. [4].

The aspect ratio of channel width-to-height, channel length-to-aeraulic diameter, baffle spacing-to-channel height ratio, and blockage ratio of baffle height-to-channel height are fixed at W/H = 1.321, L/D_h = 3.317, Pi/H = 0.972, and h/H = 0.547, respectively. The parameters studied include the entrance Reynolds number Re = 12,000, the height and spacing of baffles are fixed at h = 0.08 m and Pi = 0.142 m, respectively; whereas four various values of arc-baffle half angles were considered, θ = 30°, 45°, 60° and 75° and the heat transfer fluid is air.

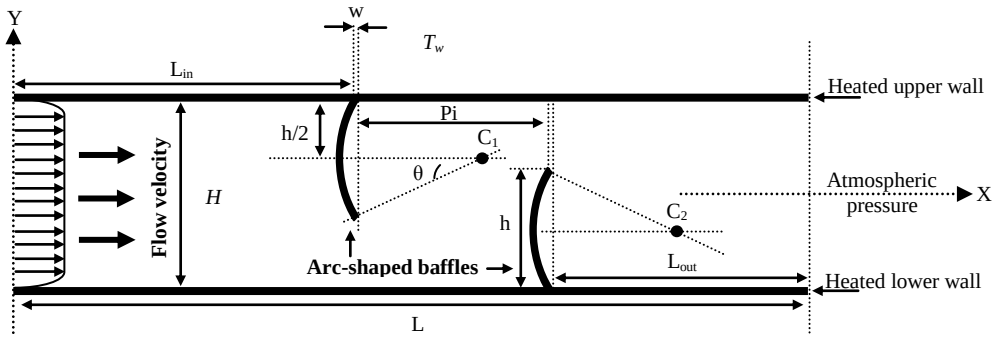

Figure1. Detail of the two-dimensional computational domain with the staggered 30° arc-upstream baffles and boundary conditions

2.2. Numerical model

The numerical model for fluid flow and heat transfer in the channel was developed under the following assumptions:

- Steady two-dimensional fluid flow and heat transfer.
- The flow is turbulent and incompressible.
- Constant fluid properties.
- Body forces and viscous dissipation are ignored.
- Negligible radiation heat transfer.

2.3. Governing equations

Based on the above assumptions, the channel flow is governed by the continuity, the Navier-stokes equations and the energy equation. In the Cartesian tensor system these equations can be written as follows:

(i) Continuity equation:

$$\frac{\partial u_j}{\partial x_j} = 0 \qquad (1)$$

(ii) Momentum equation:

$$\rho u_j \frac{\partial u_i}{\partial x_j} = -\frac{\partial P}{\partial x_i} + \frac{\partial}{\partial x_j}\left(\mu \frac{\partial u_i}{\partial x_j} - \rho \overline{u_i' u_j'}\right) \qquad (2)$$

where ρ is the fluid density (constant), P the pressure, μ dynamic viscosity, u_i and u_j are mean velocity componentsin x_i and x_j directions. u'_i and u'_j are fluctuation velocity components in x_i and x_j directions.

(iii) Energy equation:

$$\rho u_j \frac{\partial T}{\partial x_j} = \frac{\partial}{\partial x_j}\left(\left(\Gamma + \Gamma_t\right)\frac{\partial T}{\partial x_j}\right) \qquad (3)$$

where Γ and Γ_t are molecular thermal diffusivity and turbulent thermal diffusivity, respectively and are given by

$$\Gamma = \frac{\mu}{\mathrm{Pr}} \text{ and } \Gamma_t = \frac{\mu_t}{\mathrm{Pr}_t} \qquad (4)$$

with

$$-\rho \overline{u_i' u_j'} = \mu_t\left(\frac{\partial u_i}{\partial x_j} + \frac{\partial u_j}{\partial x_i}\right) - \frac{2}{3}\rho \delta_{ij} k \qquad (5)$$

$$k = \frac{1}{2}\overline{u_i' u_i'} \qquad (6)$$

$$\mu_t = \rho C_\mu \frac{k^2}{\varepsilon} \qquad (7)$$

where μ_t is the turbulent viscosity, δ_{ij} the Kroenecker delta, and k the kinetic energy of the turbulence.The steady state transport equations of the standard *k-ε* model are expressed as (Launder and Spalding [28])

$$\rho u_j \frac{\partial k}{\partial x_j} = \frac{\partial}{\partial x_j}\left[\left(\mu + \frac{\mu_t}{\sigma_k}\right)\frac{\partial k}{\partial x_j}\right] + G_k - \rho\varepsilon \qquad (8)$$

$$\rho u_j \frac{\partial \varepsilon}{\partial x_j} = \frac{\partial}{\partial x_j}\left[\left(\mu + \frac{\mu_t}{\sigma_\varepsilon}\right)\frac{\partial \varepsilon}{\partial x_j}\right] + C_{1\varepsilon}\frac{\varepsilon}{K}G_k - C_{2\varepsilon}\rho\frac{\varepsilon^2}{k} \qquad (9)$$

where

C_μ= 0.09; $C_{1\varepsilon}$= 1.44; $C_{2\varepsilon}$= 1.92; σ_k= 1.0; σ_ε= 1.3 and σ_T= 0.90 (10)

are chosen to be empirical constants [28] in the turbulence transport equations. G_k is the production rate of the kinetic energy due to the energy transfer from the mean flow to turbulence

2.4. Boundary condition

At the inlet channel (at x = 0), a uniform fluid velocity (U_{in}) was introduced while an atmospheric pressure boundary condition was applied at the exit (at x = L),

because fluid is incompressible, as presented by Demartini et al. [4]. Besides, impermeable boundary and no-slip wall conditions have been implemented over the channel walls as well as the arc-baffle surfaces. The temperatures of channel walls (T_w) and inlet fluid (T_{in}) are set as constant, which are respectively 375 and 300K, as reported by Nasiruddin and Kamran Siddiqui [8].All these thermal aerodynamic boundary conditions can be written as follows:

(i) At the intake of the computational domain(x = 0):

$$u = U_{in} \quad (11a)$$

$$v = 0 \quad (11b)$$

$$T = T_{in} \quad (11c)$$

$$k_{in} = 0.005\, U_{in}^2 \quad (11d)$$

$$\varepsilon_{in} = 0.1 k_{in}^2 \quad (11e)$$

(ii) At the channel walls (upper wall: y = H/2; lower wall: y = -H/2):

$$u = v = 0 \quad (12a)$$

$$k = \varepsilon = 0 \quad (12b)$$

$$T = T_W \quad (12c)$$

(iii) At the fluid/solid interface:

$$T_f = T_s \quad (13a)$$

$$\lambda_f \frac{\partial T_f}{\partial n} = \lambda_s \frac{\partial T_s}{\partial n} \quad (13b)$$

where *n* is the normal coordinate to the wall.

(iv) At the exit (x = L):

$$\frac{\partial u}{\partial x} = \frac{\partial v}{\partial x} = \frac{\partial T}{\partial x} = \frac{\partial k}{\partial x} = \frac{\partial \varepsilon}{\partial x} = 0 \quad (14a)$$

$$P = P_{atm} \quad (14b)$$

2.5. Thermo-hydrodynamic parameters

The Reynolds number, calculated with the aeraulic diameter D_h of the channel and the inlet velocity, $\overline{U}$ is prescribed as

$$\mathrm{Re} = \rho \overline{U} D_h / \mu \quad (15)$$

where the aeraulic diameter, D_h of the channel, is defined as:

$$D_h = 4HW / 2(H + W) \quad (16)$$

The skin friction coefficient, C_f is given by

$$C_f = \frac{\tau_w}{\frac{1}{2}\rho \overline{U}^2} \quad (17)$$

The convective heat transfer is computed by local Nusselt number, Nu_x which can be written as

$$Nu_x = \frac{h_x D_h}{\lambda_f} \quad (18)$$

where λ_f represents the thermal conductivity of fluid, and h_x is the local convective heat transfer coefficient.

3. Numerical method

The dynamic thermo-energy model of air is governed by the Reynolds averaged Navier-Stokes equations with the Standard k-ε turbulence model (Launder and Spalding [28]) and the energy equation. These equations are discretized by the Quadratic Upstream Interpolation for Convective Kinetics Differencing (QUICK) numerical scheme (Leonard and Mokhtari [29]) and Semi-Implicit Pressure Linked Equation (SIMPLE) algorithm (Patankar [30]) is implemented. A structured, quadrilateral, non-uniform mesh with refinements near the all solid boundaries in the two directions is employed (see Fig. 2). This refinement was necessary to resolve the strong velocity gradients in those regions as confirmed by Demartini et al. [4] and Nasiruddin and Kamran Siddiqui [8]. To examine the effect of the grid size on the CFD model, various node densities are verified and a mesh configuration of 245 and 95 nodes in X and Y directions, respectively, is adopted. The convergence criterion is that the normalized residuals are less than 10^{-9} for the flow equations and 10^{-12} for the energy equation.

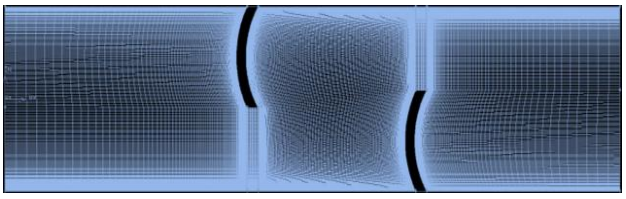

Figure 2. Grid system

Fig. 3 shows a comparison of profiles ofaxial velocity after the second arc-baffle, near the channel outlet at the reference axial station (x = 0.525, -H/2 ≤ y ≤ H/2) obtained from the present simulation for $Re=8.73\times10^4$ with those from the experiments of Demartini et al. [4]. A good agreement is observed between the numerical and experimental data.

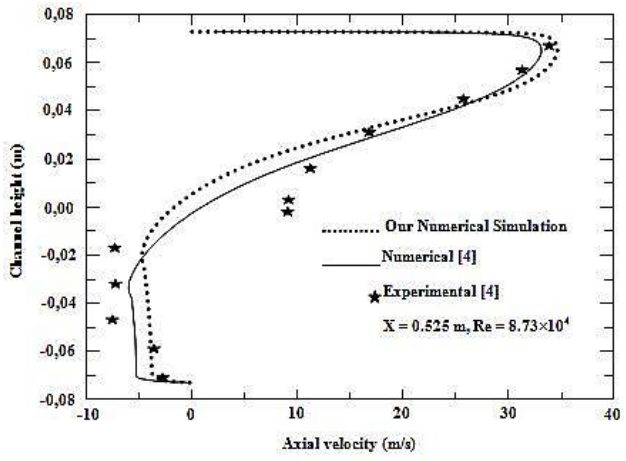

Figure 3. Validation plot of the axial velocity distribution at the axial position: (x=0.525, -H/2 ≤ y ≤ H/2).

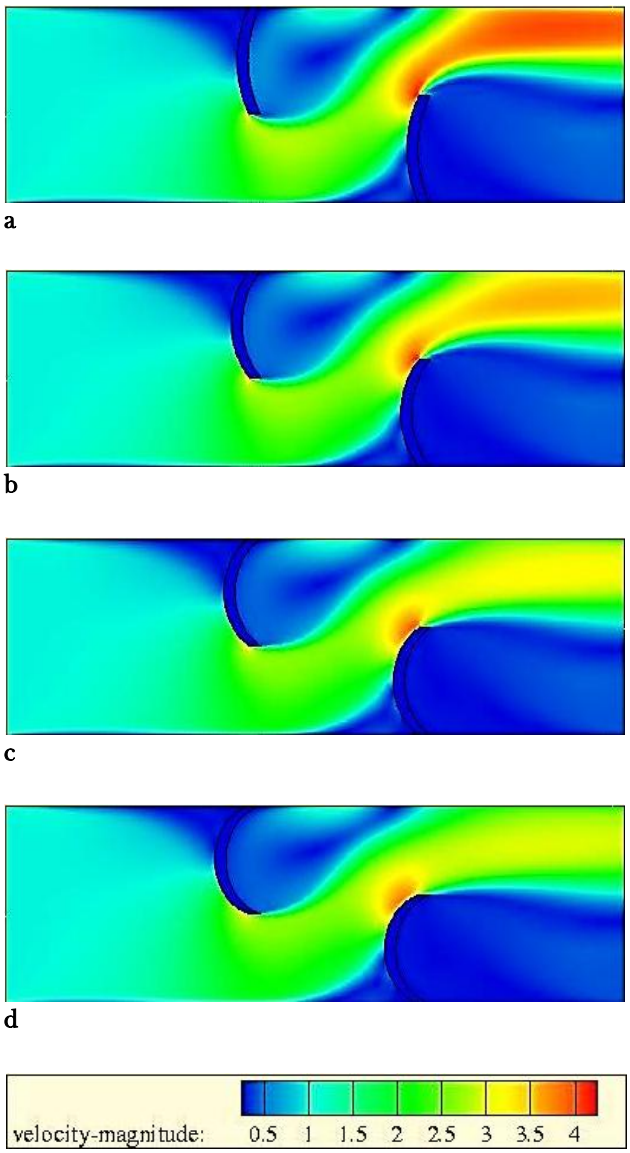

Figure 4. Velocity-magnitude fields for Re = 12,000 and (a) θ = 30°,(b) θ = 45°, (c) θ = 60°, and (d) θ = 75°.

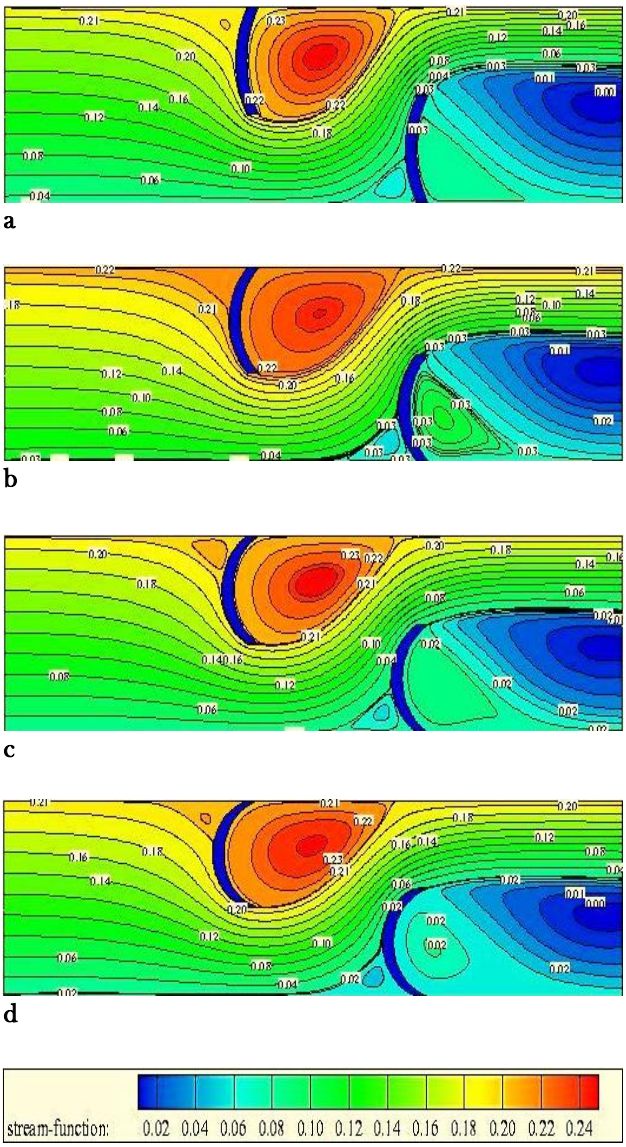

Figure 5. Streamlines for Re = 12,000 and (a) θ = 30°, (b) θ = 45°, (c) θ = 60°, and (d) θ = 75°.

4. Results and discussion

The fields of mean velocity, streamlines, profiles of axial velocityas well as the localNusselt number and skinfrictioncoefficientdistributions are shown for a constant value of the flowReynolds number, Re = 12,000.

The effect of the heated upper and lower wall-mountedarc-shaped baffle geometry on the pattern of the air flownear the solidwall is shown in Figs. 4 and 5. The contourplots in these figures present, respectively, the mean velocity fields and the streamlines for variousvaluesof angle of attack of flow by the arc-shaped baffles (θ = 30-75°) at Re = 12,000.

Computational results of profiles of the axial velocity for transverse stations x = 0.255 m and x = 0.285 m, computed behind the channel inlet, are shown in Fig. 6(a) and (b), respectively. These points are situated downstream of the leftheated upper wall-mountedarc-shapedbaffle, located at a station x = 0.218 m from the channel intake. Fig. 7(a) and (b) shows the profiles of the axial velocity at stations given by x = 0.315 m and x = 0.345 m, 0.055 m and 0.025 m before the right heated lower wall-mountedarc-baffle, respectively.

The comparison plots of axial velocity profiles after the right heated lower channel wall-mounted arc-baffle, near the outlet are calculated and analyzed along the height of the channel at x = 0.525 m (see Fig. 8).

The contour plots of temperature fields, normalized local Nusselt number, and normalized skin friction coefficient measurements were performed at the constant surface temperature conditionalong the top surface of the channel, as shown in Figs.9, 10, and 11, respectively.

In Fig. 12,the results of the variation of the thermal enhancement performance as a function of the angle of flow attack by arc-baffles inside the channel are presented.

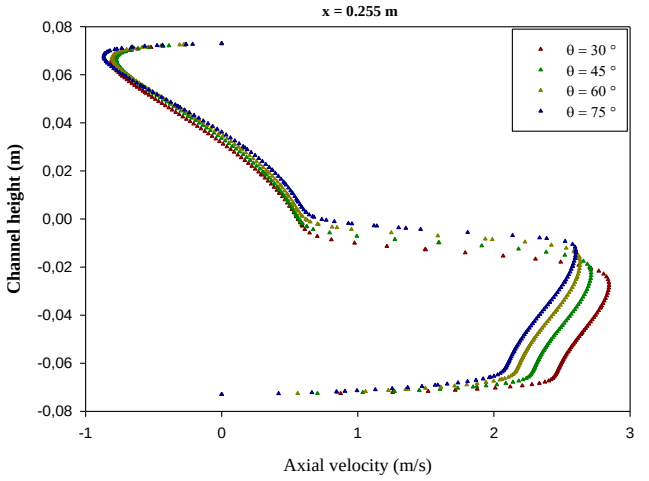

a

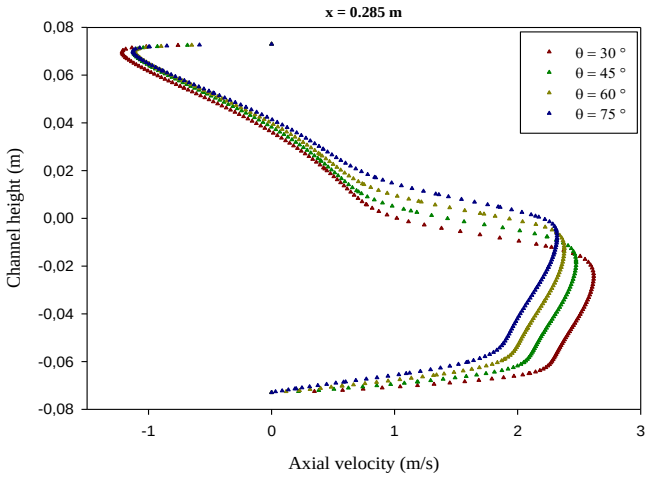

b

Figure 6. Axial velocity profiles downstream of the first arc-baffle for Re = 12,000 at (a) x = 0.255 m and (b) x = 0.285 m

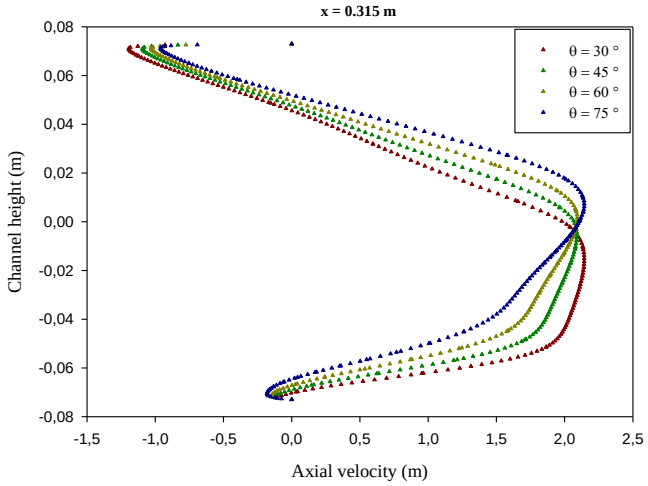

a

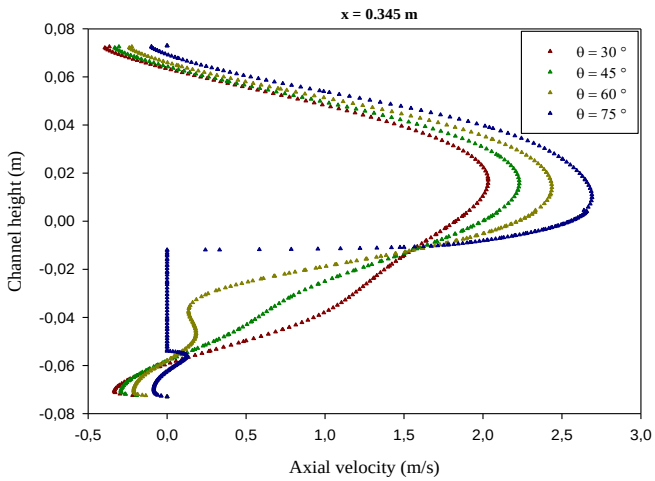

b

Figure 7. Axial velocity profiles upstream of the second arc-baffle for Re = 12,000 at (a) x = 0.315 m and (b) x = 0.345 m

The plots reveal the existence of three main regions. In the first region, just upstream of the wall-mounted arc-fins, the fluid is accelerated and arrives with an axial speed. At the approach of the upper and lower wall-attached arc-fins, the current lines are deflected. In the second region, located between the top of each arc-fin and the walls of the channel, the flow is accelerated due to the effectof cross-sectional reduction. In the third region, downstream of the arc-fins, the current lines are generated by the effect of flow expansion, thus leaving the section formed by the arc-fins and the walls. The most important phenomenon occurring in this zone is the formation of a recirculating flow whose extent is proportional to the Reynolds number, as shown in Figs. 4 and 5.

It can clearly be noticed that the values of the fluid velocity are very low in the vicinity of the two arc-fins, especially in the downstream regions; this is due to the presence of the recirculation zones. Far from these zones, the current lines become parallel, which results in the progressive development of the flow. One should also note that the axial velocity increases in the space between the end of each arc-fin and the wall of the channel.This rise in velocity is generated first by the presence of the arc-finsand then by the presence of a recycling which results in a sudden change in the direction of the flow.It is also observed that the highest values of the velocity appear near the top of the channel, with an acceleration process that begins just after the second arc-fin, thus approaching values of the order of 4.133 times of the inlet velocity, at the same Re number value, as shown in Figs. 6 and 7.

The comparison of axial velocity profiles at various angles of attack (θ)(see Figs. 6 to 8) shows that the values of theaxial velocity become higher with decreasing the values ofthe arc-fin attack angle. There is an inverse proportionality between the fluidvelocity value and the flow attack value(θ). The resultanalysis also showsthat the arc-baffle angle has an influence on the length of the flowrecirculation. The comparison of the recirculation length for different θ values shows that the 30° arc-baffle generates the longest vortex.

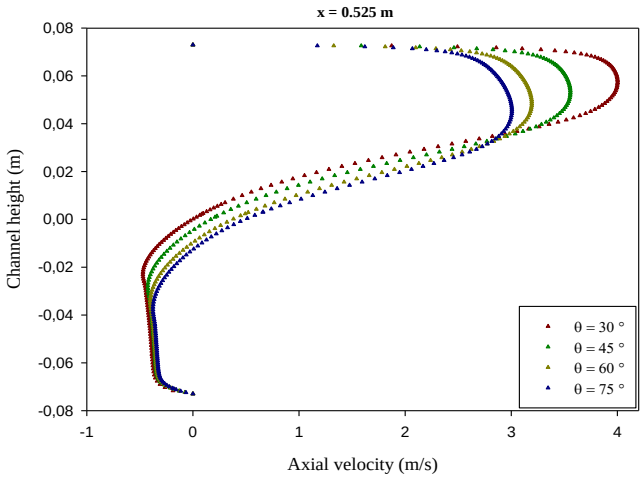

Figure 8. Axial velocity profiles after the second arc-baffle, near the channel outlet for Re = 12,000

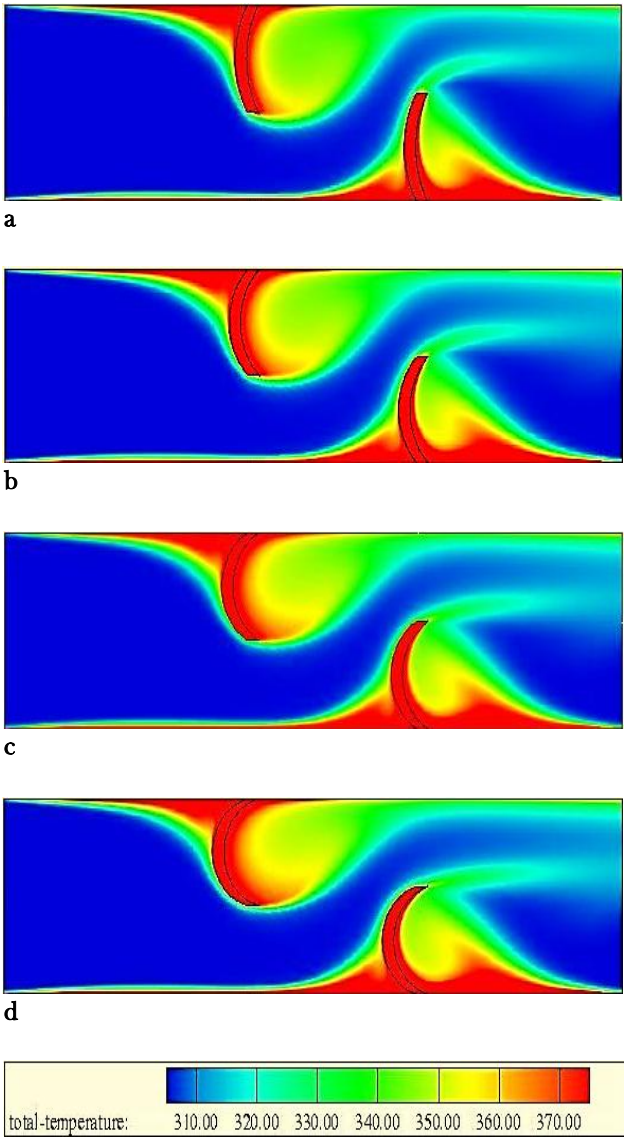

Figure 9. Temperature fields for Re = 12,000 and (a) θ = 30°,(b) θ = 45°, (c) θ = 60°, and (d) θ = 75°

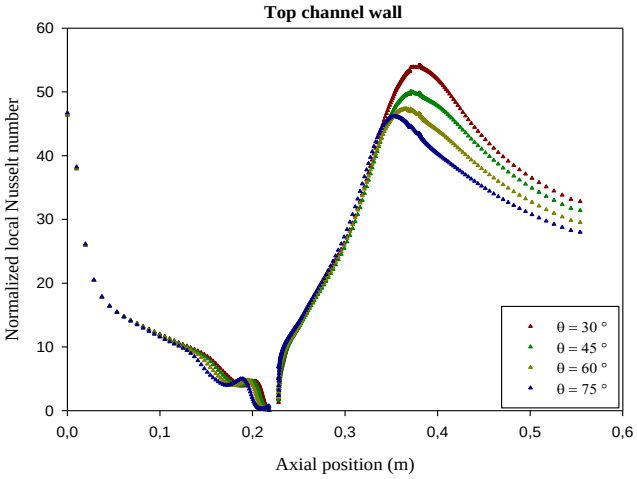

Figure 10. Axial variation of normalized local Nusselt number along the upper channel wall for various arc-baffles for Re = 12,000

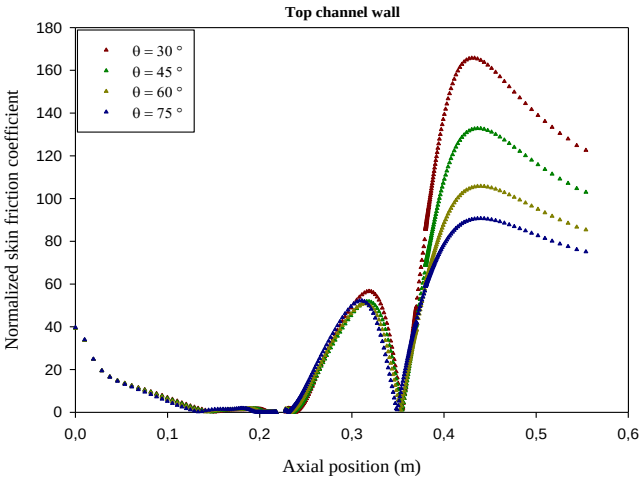

Figure 11. Axial variation of normalized skin friction coefficient along the upper channel wall for various arc-baffles for Re = 12,000

The distribution of isotherms in the given computational domain for a constant value of Reynolds number, Re = 12,000, and as given in Fig. 9, shows that the hottest areas are mostly situated near the walls and at the ends of the arc-baffles. The local Nusselt number is calculated from their definition as given in Eq. (18).The highest values of the normalized local Nusselt numberin the region opposite the right lower channel wall-mounted arc-fin are due to the strong velocity gradients in that region.The plots in this same figure alsoshow that the heat transfer rate decreases with an increase in the attack angle of air flow by the arc-shaped fins. In addition (see Fig. 10), and similarly to the results in Fig.9, the largest variations in the normalized skin friction coefficient are found near the top of the second lower channel wall-mounted arc-baffle, due to the high speeds in that region.The skin friction coefficient for air with smaller attack angle (θ) is found to be upper than that with larger θ. The Caugments with the decrease of flow attack angle (θ) and thus, the arc-shaped

fin with angle of attack of flow ofvalue of 30°provides maximum skin friction loss.

5. Conclusion

A CFD study has been carried out to investigate the turbulent forced-convection heat transfer flow and friction loss characteristics in a channel of rectangularcross section provided by two arc-shaped fins placed on the upper and lower walls. The fields of axial velocity, the profiles ofaxial velocityas well as the normalized Nusselt number and skin friction loss evaluation are presented for a constant value of flowReynolds Number at constant wall temperature condition along the top and bottom walls of the channel. The numerical result analysis shows that the augmentation of the arc-shaped fin angle of attack of flow as well as their section, by going from the 30° arc to the 75° arc, decreases the resistance to the flow and so leads to a diminution of the friction loss in the channel.

Nomenclature

Cf Skin friction coefficient
$C_{1\varepsilon}$ Constant used in the standard K-ε model
$C_{2\varepsilon}$ Constant used in the standard K-ε model
C_{μ} Constant used in the standard K-ε model
D_h Aeraulic diameter of rectangular duct, m
G_k Production of turbulent kinetic energy, m^2/s^2
H Channel height, m
h Arc-fin height, m
h_x Local convective heat transfer coefficient, $W\ m^{-2}\ K^{-1}$
k Turbulent kinetic energy, m^2/s^2
L Length of rectangular channel in x-direction, m
L_{in} Distance upstream of the first arc-fin, m
L_{out} Distance downstream of the second arc-fin, m
Nu_x Local Nusselt number
ΔP Pressure drop, Pa
P Pressure, Pa
Pi Arc-fin distance or spacing, m
P_{atm} Atmospheric pressure, Pa
Pr Molecular Prandtl number
Pr_t Turbulent Prandtl number
Re Reynolds number
T Temperature, °C
T_{in} Inlet temperature, °C
T_w Wall temperature, °C
U_{in} Inlet velocity, m/s
u Fluid velocity in x-direction, m/s
u_i, u_j Mean velocity component in x_i-, x_j-direction, m/s
u'_i u'_j Fluctuation velocity component in x_i-, x_j-direction, m/s
v Fluid velocity in y-direction, m/s
w Arc-fin width, m
x, y Cartesian coordinates, m

Greek symbols

ε Dissipation rate, m^2/s
Γ Molecular thermal-diffusivity, Kg/m.s
Γ_t Turbulent thermal-diffusivity, Kg/m.s
δ_{ij} Kronecker delta
ρ Fluid density, kg/m^3
λ_f Fluid thermal conductivity, W/m.°C
λ_s Solid thermal conductivity, W/m.°C
μ Molecular viscosity, Kg/m.s
μ_t Eddy viscosity, Kg/m.s
σ_k Turbulent Prandtl number for K-equation
σ_ε Turbulent Prandtl number for ε-equation
σ_T Turbulent Prandtl number for energy equation
θ Half attack angle of baffle, degree (°)
τ_w Wall shear stress, $Kg/s^2.m$
ϕ Stands for the dependent variables u, v, K, ε and T

Subscript

atm Atmospheric
f Fluid
i, j Refers coordinate direction vectors
in Inlet of the computational domain
out Outlet of the computational domain
s Solid
t Turbulent
w Wall
x Local

References

[1] C. Berner, F. Durst, D. M. McEligot, Trans. ASME J. Heat Transfer 106 (1984) 743-749
[2] C. H. Cheng, W.H. Huang, Int. J. Heat Mass Transfer 34 (11) (1991) 2739-2749
[3] H. Li, V. Kottke, Int. J. Heat Mass Transfer 41(10) (1998) 1303-1311
[4] L. C. Demartini, H. A. Vielmo, S. V. Möller, J. of the Braz. Soc. of Mech. Sci. & Eng. 26(2) (2004) 153-159
[5] S. S. Mousavi, K. Hooman, Energy Convers. Manag. 47 (2006) 2011-2019
[6] J. Anotoniou, G. Bergeles, ASME J. Fluids Eng. 110 (1988) 127-133
[7] S. V. Möller, L. A. M. Endres, G. Escobar,Trans.SMiRT 15 - 15thInternational Conference on Structural Mechanics in Reactor Technology7 (1999) 262-275, Seoul.
[8] Nasiruddin, M. H. Kamran Siddiqui, Int. J. Heat Fluid Flow28(2) (2007) 318-328
[9] K. Yongsiri, P. Eiamsa-ard, K. Wongcharee, S. Eiamsa-ard, Case Studies Therm. Eng. 3 (2014) 1-10
[10] R. Karwa, B. K. Maheshwari, Int. Commun. Heat Mass Transfer 36 (2009) 264-268

[11] D. Sahel, H. Ameur, R. Benzeguir, Y. Kamla, Appl. Therm. Eng. 101 (2016) 156-164
[12] P. Dutta, A. Hossain, Int. J. Heat and Fluid Flow 26 (2005) 223-232
[13] N. Guerroudj, H. Kahalerras, Energy Conv. Management 51 (2010) 505-517
[14] S. Sripattanapipat, P. Promvonge, Int. Commun. Heat Mass Transf. 36 (2009) 32-38
[15] R. Ben Slama, Solar Energy 81 (2007) 139-149
[16] A. Abene, V. Dubois, M. Le Ray, A. Ouagued, J. Food Eng. 65 (2004) 15-22
[17] S. Tamna, S. Skullong, C. Thianpong, P. Promvonge, Solar Energy 110 (2014) 720-735
[18] P. Sriromreun, C. Thianpong, P. Promvonge, Int. Commun. Heat Mass Transfer 39 (2012) 945-952
[19] K. Nanan, C. Thianpong, M. Pimsarn, V. Chuwattanakul, S. Eiamsa-ard, Appl. Therm. Eng. (2016),doi:http://dx.doi.org/10.1016/j.applthermaleng. 2016.11.153.
[20] R. Kumar, A. Kumar, R. Chauhan, M. Sethi, Case Studies Therm. Eng. 8 (2016)187-197
[21] Y. Menni, A. Azzi, C. Zidani, B. Benyoucef, J. New Technol. Mater. 6(2) (2016) 44-55
[22] Y. Menni, A. Azzi, C. Zidani, J. Eng. Science and Tech. 12(12) (2017) 3251-3273
[23] Y. Menni, A. Azzi, C. Zidani, Revue des Energies Renouvelables 20(1) (2017) 25-38
[24] Y. Menni, A. Azzi, Periodica Polytechnica Mechanical Eng. 62(1) (2018) 16-25
[25] Y. Menni, A. Azzi, J. New Tech. and Materials 7(2) (2017) 10-21
[26] Y. Menni, A. Azzi, Computational Thermal Sciences 10(3) (2018) 225–249
doi: 10.1615/ComputThermalScien.2018025026
[27] F. Merrouchi, A. Fourar, F. Massouh, D. Haddad, H. Azoui, J. New Tech. and Materials 7(1) (2017) 53-63.
[28] B. E. Launder, D. B. Spalding, Computer Meth. Appl. Mech. Eng. 3 (1974) 269-289
[29] B. P. Leonard, S. Mokhtari, Ultra-Sharp Nonoscillatory Convection Schemes for High-Speed Steady Multidimensional Flow,NASA TM 1-2568, NASA Lewis Research Center, 1990.
[30] S. V. Patankar, Numerical heat Transfer and fluid flow, McGraw-Hill, New York, 1980.